LANGMUIR Article
Cite This: Langmuir 2018, 34, 2849−2855
pubs.acs.org/Langmuir

Bimetallic Au@M (M = Ag, Pd, Fe, and Cu) Nanoarchitectures Mediated by 1,4-Phenylene Diisocyanide Functionalization

Jung-Soo Kang, Youngku Sohn, Debabrata Pradhan, and Kam Tong Leung*

WATLab and Department of Chemistry, University of Waterloo, Waterloo, Ontario N2L 3G1, Canada

Supporting Information

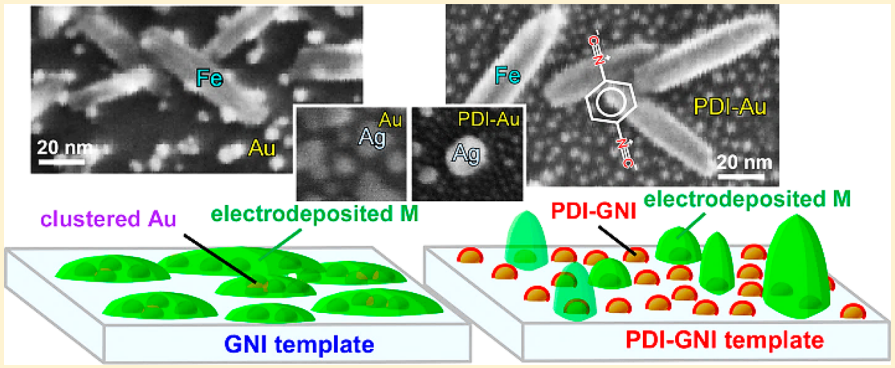

ABSTRACT: Hybridization with gold has attracted a lot of attention in many application areas such as energy, nanomedicine, and catalysts. Here, we demonstrate electrochemical hybridization of two different metals by using bare and 1,4-phenylene diisocyanide (PDI) functionalized gold nanoislands (GNIs) supported on a Si substrate. As pristine GNIs are not tightly locked on the Si surface, bimetallic Au@M (M = Ag, Pd, Fe, and Cu) core−shell type nanostructures are produced by an electric-field-induced clustering of GNIs and metal deposition. On the other hand, upon functionalization of GNIs by PDI, 3D island growth on the functionalized GNI template is observed as PDI acts as a protector against the electric-field-induced clustering. Depth-profiling X-ray photoelectron spectroscopy reveals no discernible difference in the interfacial electronic structures of hybrid metals prepared by using pristine and PDI-functionalized GNI templates. This work demonstrates a new approach to produce a secured template and to manipulate growth of hybrid nanoparticles on this template supported on a Si substrate by using electrodeposition and organic functionalization.

INTRODUCTION

Hybridization of more than two different metals has been under intense study, generally with the goal to improve its performance and/or to introduce new functionality in their applications in energy, catalysts, sensors, and drug delivery.[1−14] As a hybrid material element, gold has attracted much attention in nanoscale architecture due to its enhanced activities at the nanoscale.[11−14] A synergetic effect has commonly been observed upon introducing a second metal, including transition metals (e.g., Fe and Cu) and noble metals (e.g., Ag, Pd, and Pt).[15−25] Haldar et al. prepared bimetallic Au@Ag core−shell nanoparticles (NPs), tested catalytic reduction of 4-nitrophenol to 4-aminophenol, and found that the catalytic activity was increased with increasing the core size.[15] It was also reported that plasmonic effect of AuAg bimetallic NPs could be 20 times stronger than that of pure Au NPs.[16] Huang et al. showed that controlling the Ag shell thickness of AuAg bimetallic nanorods could give rise to change in the emission color and to region-selectable surface plasmonic effect.[17,18] Stand-alone AuPd NPs and those dispersed on graphene sheets and carbon nanotubes showed high catalytic activity for the detection of H_2O_2 and reduction of 4-nitrophenol with higher turnover frequencies, respectively.[19−21] The bimetallic catalysts were found to exhibit much higher activity than those of the monometallic Au NPs and Pd NPs. Félix-Navarro et al. prepared bimetallic PtAu NPs on multiwall carbon nanotubes and observed a superior catalytic activity for oxygen reduction.[22] Nonenzymatic glucose sensor based on bimetallic PtAu nanocatalyst showed excellent stability and selectivity.[23] Magnetic Fe_2O_3@Au core−shell structures have shown great potential for application in drug control and therapy due to its near-IR response and magnetic remote control property.[24] Wang et al. synthesized Au@Cu core−shell NPs on carbon nanofibers by using a solution method and demonstrated their application as catalysts for hydrogen production, where the core−shell structures showed enhanced electrochemical activity.[25]

In the hybridization process, morphology control during hybridization becomes increasingly difficult as the lateral size goes below 100 nm. For this reason, a more sophisticated technique of hybridization with better outcome would be highly

Received: August 2, 2017
Revised: December 15, 2017
Published: February 5, 2018

DOI: 10.1021/acs.langmuir.7b02705
Langmuir 2018, 34, 2849−2855

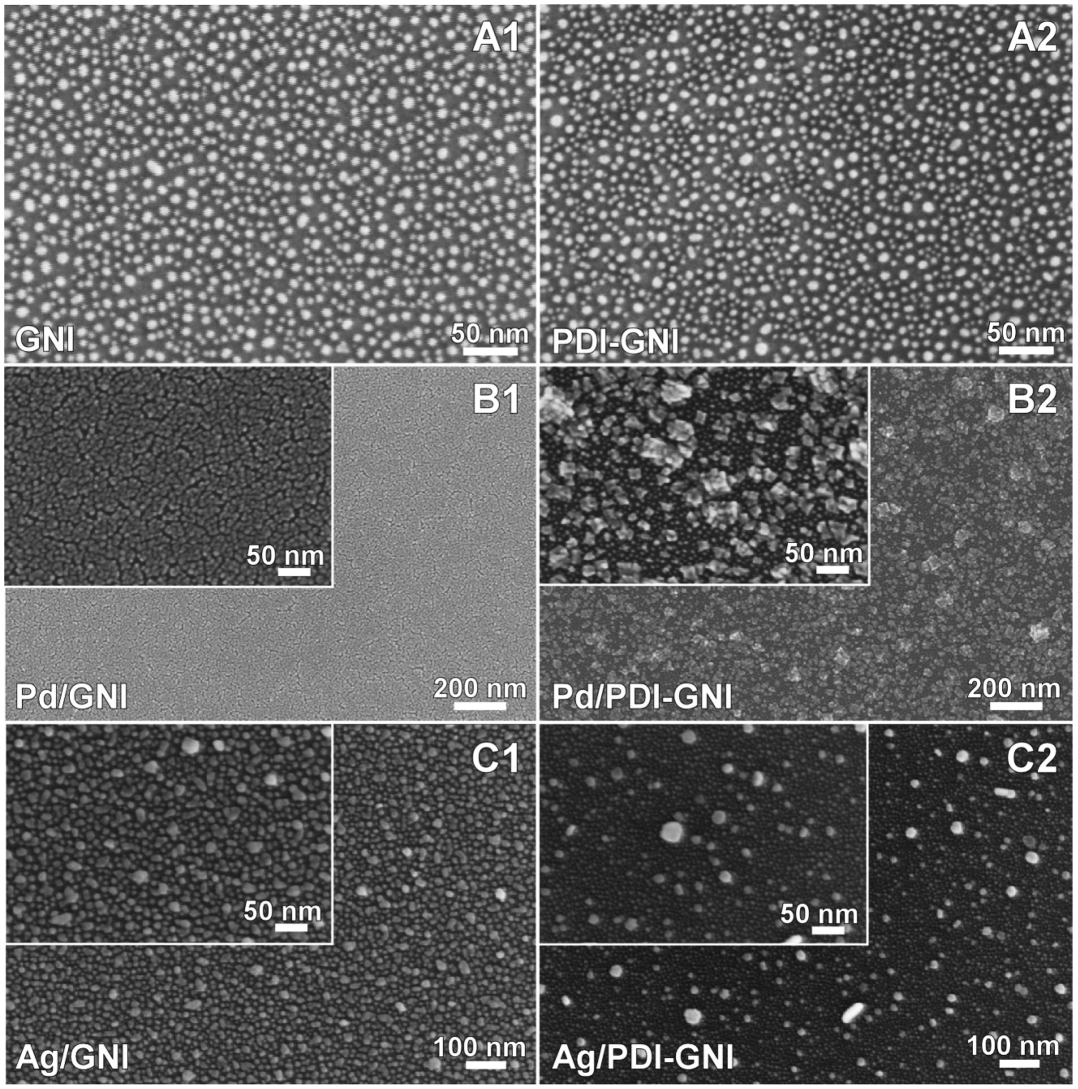

Figure 1. SEM images of (A1) bare and (A2) PDI-functionalized Au nanoisland (GNI) templates and upon (B1, B2) Pd (0.2 V for 30 s) and (C1, C2) Ag (−0.5 V for 60 s) electrodeposition onto a GNI template (B1, C1) without and (B2, C2) with PDI functionalization. Insets show SEM images of the corresponding samples at a higher magnification. Magnified SEM images of electrodeposited Ag on GNI are provided in Figure S1.

desirable. Among the various methods of preparing hybridized bimetals, electrochemical deposition has been widely used because of its many advantages, including ease of use and low cost.[26−29] In the case of nanoscale electrodeposition on a support, especially Au on Si, the bonding between the metal (Au) and the substrate (Si) should be considered carefully.[30] Because of the relatively weak Au−silicide bonding, the Au nanodeposits could experience turbulent motion caused by the externally applied electric field, which could significantly affect the spatial distribution of the nanodeposits and the resulting nanotemplate.

As nanoscale architecture developed by surface engineering is of great interest, surface functionalization by organic adspecies has become the method of choice to modify a surface.[31,32] In this work, 1,4-phenylene diisocyanide (PDI, $^{-}C{\equiv}N^{+}{-}C_6H_4{-}N^{+}{\equiv}C^{-}$) is selected as a coordinating agent between GNI and an overlayer electrodeposited metal. The PDI is one of the simplest molecules that has an isocynide group and it is well-known that an isocynide group could form σ-bonding with metal elements.[32−36] In particular, PDI reacts with gold, leading to the formation of $-(Au{-}PDI)_n-$ oligomers.[34] Here, we demonstrate that metal growth on a GNI-decorated substrate can be altered by prefunctionalization of the GNI template with and without PDI. Bare GNIs on a Si substrate can be dislodged by the electric field generated by the applied potentials during electrodeposition of the selected metals, and they become clustered together. This field-driven disruption could be prevented by PDI functionalization on GNIs. The locking of GNIs on the surface by PDI provides an important technique for constructing nanoscale architectures, especially for assuring that bimetals can be uniformly electrodeposited over a large area to produce a large template.

■ EXPERIMENTAL SECTION

Materials. 1,4-Phenylene diisocyanide ($C_6H_4(NC)_2$, 97%), toluene ($C_6H_5CH_3$, 99.8%), silver nitrate ($AgNO_3$, ≥99.0%), iron(III) chloride hexahydrate ($FeCl_3{\cdot}6H_2O$, 97%), copper sulfate pentahydrate ($CuSO_4{\cdot}5H_2O$, ≥98.0%), palladium chloride ($PdCl_2$, 99%) and sodium perchlorate monohydrate ($NaClO_4{\cdot}H_2O$, 98%) were purchased from Sigma-Aldrich and used without further purification.

Preparation of GNI and Bimetallic Nanostructures. GNIs supported on a p-type Si(100) substrate (single-side-polished, 15 × 2.5 mm^2 and 0.4 mm thick) were prepared by sputter-deposition of Au

DOI: 10.1021/acs.langmuir.7b02705
Langmuir 2018, 34, 2849−2855

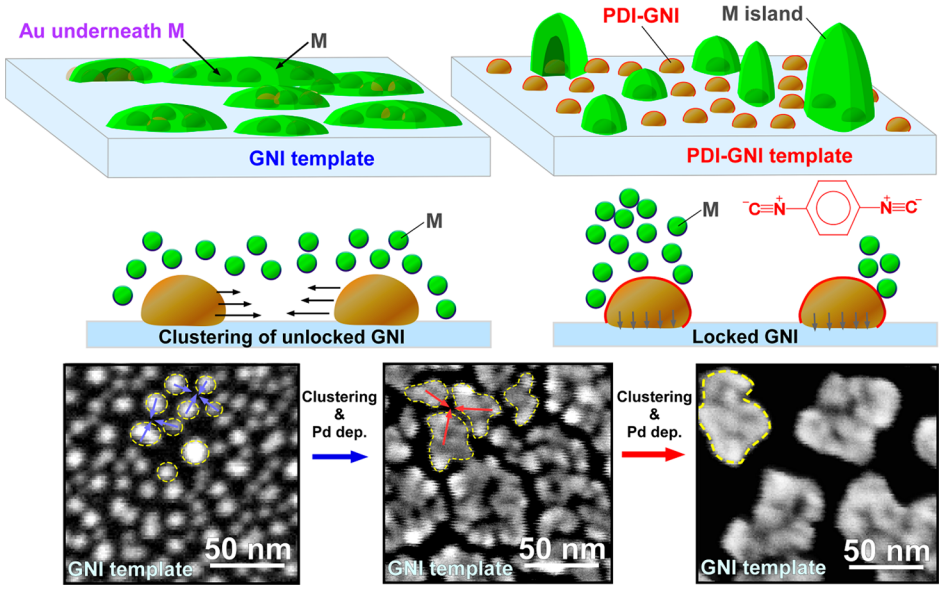

Figure 2. Growth models of electrodeposited metal on bare (top left) and PDI-functionalized (top right) GNI templates. Bare GNIs (middle left) are highly mobile on the Si surface and become clustered together under the effect of an applied potential, while PDI-functionalized GNIs (middle right) are apparently locked down by the PDI overlayer (red line) and are strongly bonded on the surface. The SEM images (lower) illustrate changes in the morphology for Pd deposition on a bare GNI template with increasing electrodeposition time.

using a magnetron sputter-coater (Denton Desk II), followed by thermal annealing at 450 °C for 1 h in a conventional (air medium) oven. For PDI functionalization, a bare GNI template (or a Au thin-film substrate obtained by magnetron-sputtering without the postannealing) was dipped in a 1 mM PDI toluene solution for 24 h followed by thoroughly washing with toluene to remove physisorbed multilayer PDI. The selected metals were electrodeposited on a bare or a PDI-functionalized GNI template potentiostatically by amperometry in a three-electrode cell with a CH Instruments 660A electrochemical workstation. A standard Ag/AgCl electrode and a platinum wire were used as the reference and counter electrodes, respectively. For metal electrodeposition on a GNI template, we used a 10 mM deoxygenated aqueous solution of $AgNO_3$, $FeCl_3$, or $CuSO_4$ along with 100 mM $NaClO_4$ as the supporting electrolyte. For Pd deposition, we used a 0.1 mM solution of $PdCl_2$ as the electrolyte. After the electrodeposition, we thoroughly rinsed the samples with filtered deionized water (18.2 MΩ cm resistivity) and dried under nitrogen stream before XPS and SEM analysis.

Characterization. Surface morphology of the resulting nanodeposits was examined by field-emission scanning electron microscopy (FE-SEM) using a Zeiss LEO 1530 microscope. The corresponding chemical states were analyzed by X-ray photoelectron spectroscopy (XPS) as a function of Ar^+ ion sputtering time in a Thermo-VG Scientific ESCALab 250 Microprobe equipped with a hemispherical analyzer and a monochromatic Al Kα X-ray source (1486.6 eV). For depth profiling studies, sputtering was rastered over a sample area of 2 × 2 mm^2 at an ion beam energy of 3 keV and a sample current density of 102 nA/mm^2.

RESULTS AND DISCUSSION

Pd and Ag Electrodeposition. Figure 1 shows the SEM images of two different metals (Pd and Ag) hybridized with GNIs by electrodeposition with and without PDI functionalization. Before electrodeposition, GNIs with sizes less than 10 nm are uniformly distributed on a Si support (Figures 1A1 and 1A2). The GNIs show no visible difference before and after PDI functionalization. Without PDI functionalization, the as-deposited metal overlayers of Pd (Figure 1B1) and Ag (Figure 1C1) are found to completely cover the GNIs uniformly, without any area of the GNIs exposed. The resulting hybrid islands generally become much larger than the bare GNIs, which indicates that each hybrid island covers two or more GNIs. When compared to the bare GNI template, the number density of the islands has been discernibly reduced, and the average size of the islands has concomitantly become larger. For electrodeposition on the PDI-functionalized GNI template (Figures 1B2 and 1C2), the islands become very nonuniform and significantly larger islands appear on individual GNIs. For electrodeposited metal on the GNI template, we confirm the presence of electrodeposited metal by energy dispersive X-ray (EDX) analysis (see Figure S1, Supporting Information).

Unlocked and Locked Au Nanoislands and the Role of PDI. We illustrate a growth mechanism proposed for electrodeposited metal on bare and PDI-functionalized GNI templates in Figure 2. For the bare GNI template, our hypothesis is that once nucleation of the metal (Pd or Ag) occurs on a bare GNI, the metal seed could migrate and eventually merge with another seed on the original or another GNI, as shown schematically in Figure 2. At the same time, the electrochemical action also induces migration of the entire GNI, which also results in the transport of the metal seeds already deposited on the GNIs. The field-induced migration therefore produces both seed-to-seed and GNI-to-GNI gradual hybridization, which cause the GNIs to become fully covered by the metal overlayer. With increasing deposition time, the GNI−metal core−shell nanostructure becomes larger, as shown in the SEM images for Pd growth evolution on the bare GNI template (Figure 2). To further support our proposed model of electric field-induced aggregation and core−shell formation, we provide SEM images for Pd electrodeposited on GNIs prepared at various applied potentials and with different amounts of time in Figure S2.

For the PDI-functionalized GNI template, the metal overlayer appears to follow the Stranski−Krastanov growth mode, where a metal seed on a GNI grows in size, without merging with another seed on other GNI, to form the overlayer that eventually covers the entire PDI-functionalized GNI

DOI: 10.1021/acs.langmuir.7b02705
Langmuir 2018, 34, 2849−2855

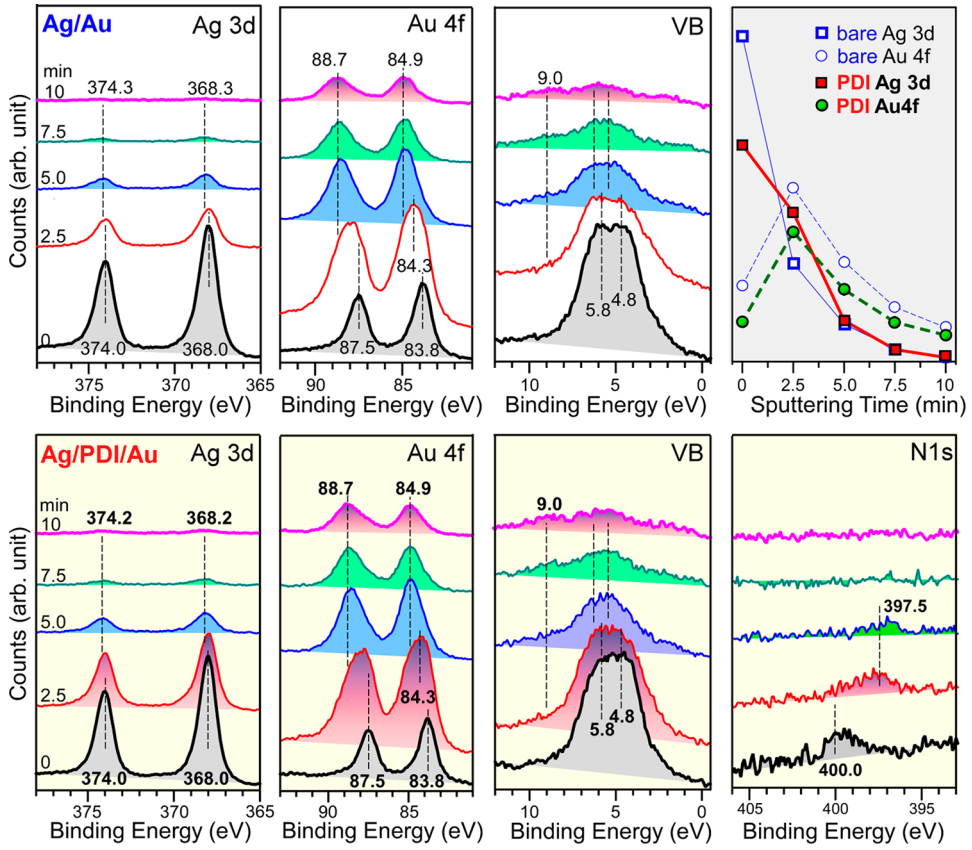

Figure 3. XPS spectra of Ag 3d, Au 4f, N 1s, and valence band (VB) regions of Ag as-electrodeposited on Au nanoislands without (upper) and with (lower) PDI functionalization and with increasing Ar ion sputtering time to 10 min. Upper right panel displays the corresponding changes in Ag 3d and Au 4f peak intensities with sputtering time (after appropriate consideration of the relative sensitivity factors: Au 4f = 4.95 and Ag 3d = 5.2).

(Figure 2, top right). For bare GNI template, growth of the overlayer metal can be explained by the Frank–van der Merwe (or layer-by-layer) growth mode and is accompanied by GNI clustering. On the basis of our XPS results for the PDI-functionalized GNI template (Figure S3), we suggest that one –NC group of the PDI molecule is bound to the Au atoms on a GNI by linear σ-bonding, with the other terminal –NC group remaining free. This is in good accord with the literature.[35,36] The positive metal ions are more easily attracted to the negatively charged $-^{+}N{\equiv}C^{-}$ group to form a complex before undergoing chemical reduction.[37] It should be noted that the growth of the metal (Ag and Pd) seed on the bare region of the Si substrate (not covered by GNIs) is limited because the Si surface is oxidized and less conductive than the GNIs. In a separate experiment, we deposit PDI directly on a bare Si substrate. The lack of detectable N 1s XPS signal for a bare Si substrate functionalized by PDI therefore confirms that PDI does not attach well on the bare part of the Si substrate.

For the viewpoint of application, electrocatalytic activities of a bare Si substrate as well as GNI substrates without and with PDI functionalization are evaluated by cyclic voltammetry in a 0.1 M sodium perchlorate aqueous solution (Figure S4). Evidently, the PDI-functionalized GNI template exhibits a higher current than the bare GNI template, which is due to a larger GNI surface area resulting from PDI functionalization that prevents field-induced aggregation of GNIs.

Depth-Profiling XPS of Ag on GNI and PDI-Functionalized GNI Templates. We have examined the difference in chemical-state composition between the hybridized metals prepared on GNI templates with and without PDI functionalization and their interfacial nature by using depth-profiling XPS. In Figure 3, we show typical XPS data for Ag–Au hybridized metals electrodeposited with and without PDI functionalization, for which the corresponding XPS survey scans show the presence of Ag, Au, C, and O (Figure S5) and no impurity peaks. On the other hand, nitrogen species are only observed in the region scans for the PDI-functionalized GNI template (Figure 3). For the as-prepared samples, the Ag 3d peaks appear more prominent than the Au 4f features, consistent with Ag being the top layer. Sputtering for 10 min is sufficient to completely remove all the Ag, exposing the Au $4f_{7/2}$ Au–silicide feature at 84.9 eV. In particular, the Ag $3d_{5/2}$ (Ag $3d_{3/2}$) peak at 368.0 eV (374.0 eV), corresponding to the metallic Ag overlayer, becomes diminished with increasing sputtering time, and it shifts slightly by 0.2 eV to a higher binding energy with no change in the spin–orbit splitting (of 6.0 eV). The binding energy shift is likely due to the support, quantum size, and/or alloy effect.[30] On the other hand, the Au $4f_{7/2}$ (Au $4f_{5/2}$) peak at 83.8 eV (87.5 eV) is shifted by 0.5 eV to a higher binding energy upon sputtering for 2.5 min. It should be noted that the slightly lower Au 4f binding energy value found for the as-prepared samples than that of bulk metallic Au (by 0.2 eV) could be attributed to Ag–Au nanoalloy formation.[38] Upon 2.5 min sputtering, the Au 4f peaks shift by 0.5 eV and become much broader, while the Ag 3d peaks show no discernible change in the peak position or the width. We attribute this binding energy shift to Au–Si interaction caused by the Si support and/or Au silicide alloy formation. The broad peak can therefore be attributed to a mixture of contributions from metallic Au and Si support/silicide (Figure

DOI: 10.1021/acs.langmuir.7b02705
Langmuir 2018, 34, 2849–2855

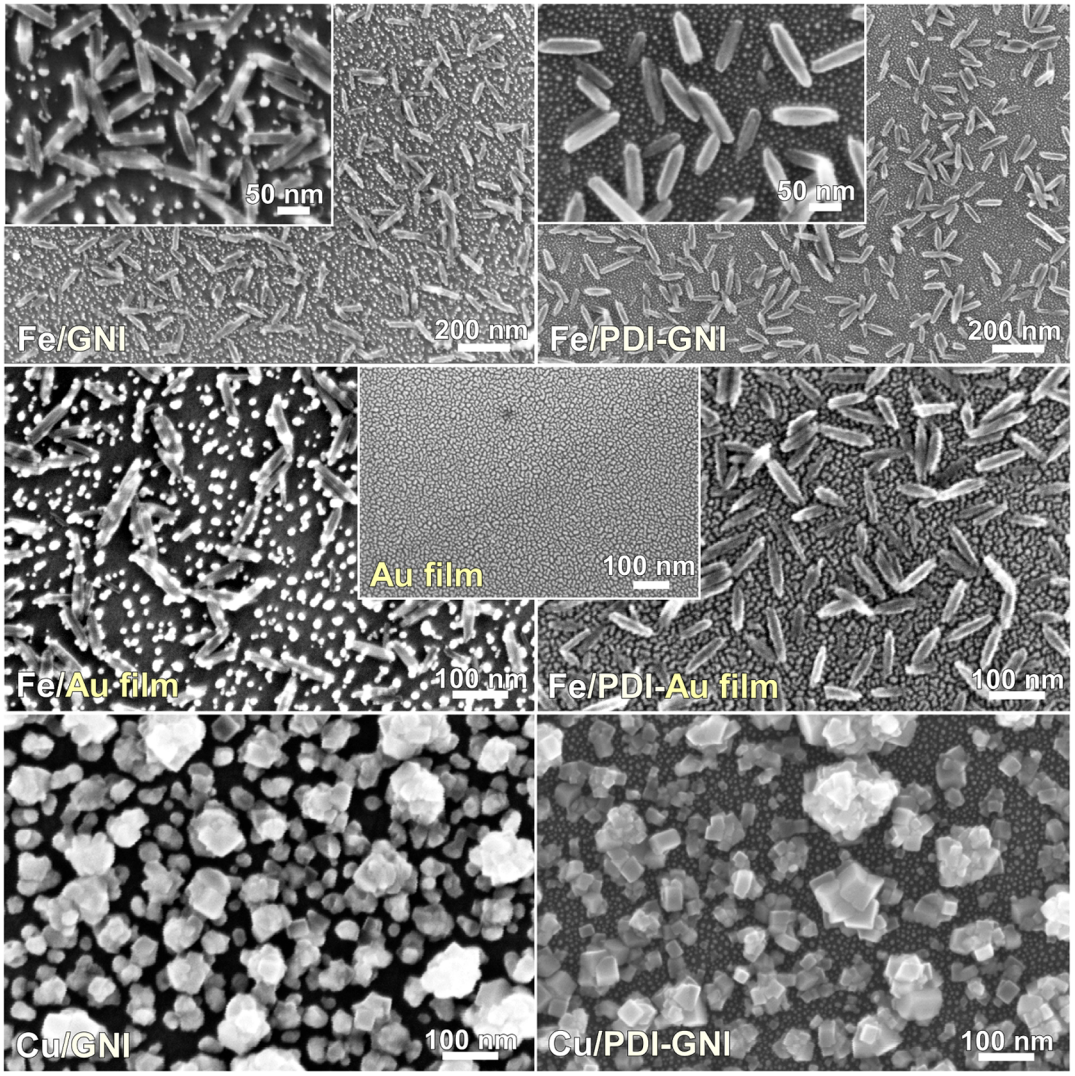

Figure 4. SEM images of bare (left column) and PDI-functionalized (right column) GNI (top) templates upon Fe (top) and Cu (one cyclic voltammetry from −1.5 to 1.5 V) electrodeposition (bottom). Middle panels show Fe (−1.0 V for 60 s) electrodeposition on a Au thin-film substrate without and with PDI functionalization, with the pristine Au film shown as inset.

S6). Upon 10.0 min sputtering, Ag is completely removed, and the only remaining Au $4f_{7/2}$ (Au $4f_{5/2}$) peak is located at 84.9 eV (88.7 eV), corresponding to the Au silicide formed at the Au−Si interface. We also observe a broad N 1s peak at 400.0 eV, which is attributed to NC−Au bonding.[35,36] The N 1s peak is found to shift to a lower binding energy with sputtering, which suggests plausible dissociation of the NC group from the aromatic ring to form a chemisorbed −N═C⟨ (imine)-type bond on Au.[35,39] The depth profiles are also shown in Figure 3. The Au/Ag ratios are 0.24 and 0.19 for the as-prepared Ag nanodeposits on bare GNI and PDI-GNI templates, respectively. The smaller Au/Ag ratio for the PDI-GNI sample is likely due to the presence of PDI chemisorbed on the GNI template. Upon 2.5 min sputtering, the Ag 3d intensity decreases while the Au 4f intensity increases, as expected. However, the decrease in the Ag 3d intensity for the bare GNI template is more drastic, reflecting a more uniform Ag layer. Upon sputtering for more than 2.5 min, the Ag 3d and Au 4f intensities are found to both gradually decrease in a similar fashion for the bare GNI and PDI−GNI samples.

Fe and Cu Electrodeposition on the GNI and PDI−GNI Templates. To further confirm the electric-field-induced clustering effect of pristine gold nanoislands on a Si substrate and the lockdown effect of PDI on GNIs, we conduct electrodeposition studies of iron and copper on the GNI templates (Figure 4). The deposited rice-shaped Fe NPs are commonly found to be 100−150 nm long and ∼30 nm thick. For the PDI-functionalized GNI template, the Fe nanorice NPs are deposited without significantly impacting the GNI template, with the GNIs clearly visible on the Si substrate. For Cu deposition on the PDI-functionalized GNI template, the GNIs are similarly unaffected by the electrodeposition. However, for Fe electrodeposition on the bare GNI template and in spite of Fe not engulfing the GNI, significant clustering and movement of bare GNIs are clearly evident. For Cu electrodeposition on the bare GNI template, the GNIs appear to become larger due to Au clustering and to the Cu deposition on GNIs, as similarly observed for Ag and Pd (Figures 1 and 2). To further show the movement and clustering of GNIs, we employ bare and PDI-functionalized thin Au films as the substrates and repeat the electrodeposition experiment of Fe (Figure 4, middle panel). Evidently, the PDI-functionalized Au film substrate shows no critical impact upon Fe deposition. On the other hand, the bare Au film substrate has remarkably changed to Au NPs upon Fe

DOI: 10.1021/acs.langmuir.7b02705
Langmuir 2018, 34, 2849−2855

deposition. This is a significant result, and it confirms that the employed electric field could induce clustering due to the weak interfacial bonding of Au−Si. Depth-profiling XPS results show that Fe nanorice NPs consist of three layers of different oxidation states—Fe (core), FeO (midshell), and an outermost thin Fe_2O_3 and/or FeOOH skin[40,41]—and that electrodeposited Cu nanodeposits on GNI correspond to metallic Cu cores individually covered by a Cu_2O shell with a CuO outermost skin.[28,42]

CONCLUSIONS

In summary, we report the first observation of an electric-field-induced electrochemical clustering of GNIs on a Si surface. Using the field-induced gold clustering effect and the preferred electrodeposition on GNIs, we develop supported bimetallic Au@M (M = Ag, Pd, Fe, and Cu) core−shell nanostructures and examine their interfacial structures by depth-profiling XPS. The bonding between Au nanoislands and the Si support is governed by formation of Au silicide. As this bonding is inherently weaker for smaller GNIs because of the smaller contact area between Au and Si, such interaction could be sufficiently small to be disrupted and indeed overcome by the external electric field density during an electrochemical action, causing turbulent motion of the GNIs. This provides the mechanism for GNIs to aggregate into larger islands and to be selectively encapsulated by the overlaying metal atoms. We further show that we could, in effect, turn off this field-induced GNI clustering by a simple surface modification using 1,4-phenylene diisocyanide or PDI ($^{-}C{\equiv}N^{+}-C_6H_4-N^{+}{\equiv}C^{-}$), where the PDI linker acts as a protector. Remarkably, PDI functionalization changes neither the chemical states nor their compositions in the formation of Au−metal hybrid materials. Organic functionalization of GNIs by PDI on a Si support could therefore play a crucial role in hybridization of two different metals. Such a template with "locked" or "unlocked" GNIs could potentially offer a wide range of applications, including catalysis and sensing applications.

ASSOCIATED CONTENT

Supporting Information

The Supporting Information is available free of charge on the ACS Publications website at DOI: 10.1021/acs.langmuir.7b02705.

EDX of Ag on a GNI template, SEM images of Pd on a GNI template, XPS spectra of a PDI-functionalized GNI template, survey XPS spectra of Ag/GNI and Ag/PDI/GNI, and Au 4f spectra of a GNI template before and after sputtering (PDF)

AUTHOR INFORMATION

Corresponding Author

*E-mail: tong@uwaterloo.ca (K.T.L.).

ORCID

Debabrata Pradhan: 0000-0003-3968-9610

Kam Tong Leung: 0000-0002-1879-2806

Present Addresses

Y.S.: Department of Chemistry, Chungnam National University, Daejeon 34134, Republic of Korea.

D.P.: Materials Science Center, Indian Institute of Technology, Kharagpur, West Bengal 721 302, India.

Notes

The authors declare no competing financial interest.

ACKNOWLEDGMENTS

This work was supported by the Natural Sciences and Engineering Research Council of Canada.

REFERENCES

(1) Wee, K.-R.; Sherman, B. D.; Brennaman, M. K.; Sheridan, M. V.; Nayak, A.; Alibabaei, L.; Meyer, T. J. An Aqueous, Organic Dye Derivatized SnO_2/TiO_2 Core/Shell Photoanode. *J. Mater. Chem. A* **2016**, *4*, 2969−2975.

(2) Kongkanand, A.; Subramanian, N. P.; Yu, Y.; Liu, Z.; Igarashi, H.; Muller, D. A. Achieving High-Power PEM Fuel Cell Performance with an Ultralow-Pt-Content Core−Shell Catalyst. *ACS Catal.* **2016**, *6*, 1578−1583.

(3) Zhang, Z.-C.; Xu, B.; Wang, X. Engineering Nanointerfaces for Nanocatalysis. *Chem. Soc. Rev.* **2014**, *43*, 7870−7886.

(4) Sheppard, T. L.; Price, S. W. T.; Benzi, F.; Baier, S.; Klumpp, M.; Dittmeyer, R.; Schwieger, W.; Grunwaldt, J.-D. In Situ Multimodal 3D Chemical Imaging of a Hierarchically Structured Core@Shell Catalyst. *J. Am. Chem. Soc.* **2017**, *139*, 7855−7863.

(5) Jiang, J.; Li, Y.; Liu, J.; Huang, X.; Yuan, C.; Lou, X. W. Recent Advances in Metal Oxide-based Electrode Architecture Design for Electrochemical Energy Storage. *Adv. Mater.* **2012**, *24*, 5166−5180.

(6) Luc, W.; Collins, C.; Wang, S.; Xin, H.; He, K.; Kang, Y.; Jiao, F. Ag−Sn Bimetallic Catalyst with a Core−Shell Structure for CO_2 Reduction. *J. Am. Chem. Soc.* **2017**, *139*, 1885−1893.

(7) Zhang, S.; Hao, Y.; Su, D.; Doan-Nguyen, V. V. T.; Wu, Y.; Li, J.; Sun, S.; Murray, C. B. Monodisperse Core/Shell Ni/FePt Nanoparticles and Their Conversion to Ni/Pt to Catalyze Oxygen Reduction. *J. Am. Chem. Soc.* **2014**, *136*, 15921−15924.

(8) Doane, T. L.; Burda, C. The Unique Role of Nanoparticles in Nanomedicine: Imaging, Drug Delivery and Therapy. *Chem. Soc. Rev.* **2012**, *41*, 2885−2911.

(9) Zhang, Y.; Li, J.; Rong, H.; Tong, X.; Wang, Z. Self-Template Synthesis of Ag−Pt Hollow Nanospheres as Electrocatalyst for Methanol Oxidation Reaction. *Langmuir* **2017**, *33*, 5991−5997.

(10) Mayorga-Martinez, C. C.; Guix, M.; Madrid, R. E.; Merkoçi, A. Bimetallic Nanowires as Electrocatalysts for Nonenzymatic Real-time Impedancimetric Detection of Glucose. *Chem. Commun.* **2012**, *48*, 1686−1688.

(11) Amram, D.; Rabkin, E. Core(Fe)−Shell(Au) Nanoparticles Obtained from Thin Fe/Au Bilayers Employing Surface Segregation. *ACS Nano* **2014**, *8*, 10687−10693.

(12) Zhang, L.; Xie, Z.; Gong, J. Shape-controlled Synthesis of Au−Pd Bimetallic Nanocrystals for Catalytic Applications. *Chem. Soc. Rev.* **2016**, *45*, 3916−3934.

(13) Aguilar-Tapia, A.; Delannoy, L.; Louis, C.; Han, C. W.; Ortalan, V.; Zanella, R. Selective Hydrogenation of 1,3-butadiene Over Bimetallic Au-Ni/TiO_2 Catalysts Prepared by Deposition-precipitation with Urea. *J. Catal.* **2016**, *344*, 515−523.

(14) Sankar, M.; He, Q.; Dawson, S.; Nowicka, E.; Lu, L.; Bruijnincx, P. C. A.; Beale, A. M.; Kiely, C. J.; Weckhuysen, B. M. Supported Bimetallic Nano-alloys as Highly Active Catalysts for The One-pot Tandem Synthesis of Imines and Secondary Amines from Nitrobenzene and Alcohols. *Catal. Sci. Technol.* **2016**, *6*, 5473−5482.

(15) Haldar, K. K.; Kundu, S.; Patra, A. Core-Size-Dependent Catalytic Properties of Bimetallic Au/Ag Core−Shell Nanoparticles. *ACS Appl. Mater. Interfaces* **2014**, *6*, 21946−21953.

(16) Liu, K.; Bai, Y.; Zhang, L.; Yang, Z.; Fan, Q.; Zheng, H.; Yin, Y.; Gao, C. Porous Au−Ag Nanospheres with High-Density and Highly Accessible Hotspots for SERS Analysis. *Nano Lett.* **2016**, *16*, 3675−3681.

(17) Dai, L.; Song, L.; Huang, Y.; Zhang, L.; Lu, X.; Zhang, J.; Chen, T. Bimetallic Au/Ag Core−Shell Superstructures with Tunable Surface Plasmon Resonance in the Near-Infrared Region and High Perform-

DOI: 10.1021/acs.langmuir.7b02705
Langmuir 2018, 34, 2849−2855

ance Surface-Enhanced Raman Scattering. *Langmuir* **2017**, *33*, 5378−5384.
(18) Huang, Y.; Ferhan, A. R.; Kim, D.-H. Tunable Scattered Colors Over a Wide Spectrum from a Single Nanoparticle. *Nanoscale* **2013**, *5*, 7772−7775.
(19) Huang, Y.; Ferhan, A. R.; Dandapat, A.; Yoon, C. S.; Song, J. E.; Cho, E. C.; Kim, D.-H. A Strategy for the Formation of Gold−Palladium Supra-Nanoparticles from Gold Nanoparticles of Various Shapes and Their Application to High-Performance H_2O_2 Sensing. *J. Phys. Chem. C* **2015**, *119*, 26164−26170.
(20) Chen, X.; Cai, Z.; Chen, X.; Oyama, M. AuPd bimetallic nanoparticles decorated on graphene nanosheets: their green synthesis, growth mechanism and high catalytic ability in 4-nitrophenol reduction. *J. Mater. Chem. A* **2014**, *2*, 5668−5674.
(21) Deng, W.; Chen, J.; Kang, J.; Zhang, Q.; Wang, Y. Carbon Nanotube-supported Au−Pd Alloy with Cooperative Effect of Metal Nanoparticles and Organic Ketone/quinone Groups as A Highly Efficient Catalyst for Aerobic Oxidation of Amines. *Chem. Commun.* **2016**, *52*, 6805−6808.
(22) Félix-Navarro, R. M.; Beltrán-Gastélum, M.; Reynoso-Soto, E. A.; Paraguay-Delgado, F.; Alonso-Nuñez, G.; Flores-Hernández, J. R. Bimetallic Pt−Au Nanoparticles Supported on Multi-wall Carbon Nanotubes as Electrocatalysts for Oxygen Reduction. *Renewable Energy* **2016**, *87*, 31−41.
(23) Nantaphol, S.; Watanabe, T.; Nomura, N.; Siangproh, W.; Chailapakul, O.; Einaga, Y. Bimetallic Pt−Au nanocatalysts electrochemically deposited on boron-doped diamond electrodes for nonenzymatic glucose detection. *Biosens. Bioelectron.* **2017**, *98*, 76−82.
(24) Li, W. P.; Liao, P. Y.; Su, C. H.; Yeh, C. S. Formation of Oligonucleotide-gated Silica Shell-coated Fe_3O_4 Au Core-shell Nanotrisoctahedra for Magnetically Targeted and Near-infrared Light-responsive Theranostic Platform. *J. Am. Chem. Soc.* **2014**, *136*, 10062−10075.
(25) Wang, J.; Zhu, H.; Yu, D.; Chen, J.; Chen, J.; Zhang, M.; Wang, L.; Du, M. Engineering the Composition and Structure of Bimetallic Au−Cu Alloy Nanoparticles in Carbon Nanofibers: Self-Supported Electrode Materials for Electrocatalytic Water Splitting. *ACS Appl. Mater. Interfaces* **2017**, *9*, 19756−19765.
(26) Crespo, M. T. A. Review of Electrodeposition Methods for The Preparation of Alpha-radiation Sources. *Appl. Radiat. Isot.* **2012**, *70*, 210−215.
(27) Sohn, Y.; Pradhan, D.; Leung, K. T. Electrochemical Pd Nanodeposits on a Au Nanoisland Template Supported on Si(100): Formation of Pd−Au Alloy and Interfacial Electronic Structures. *ACS Nano* **2010**, *4*, 5111−5120.
(28) Sohn, Y.; Pradhan, D.; Zhao, L.; Leung, K. T. Anomalous Oxidation Resistance of "Core-Only" Copper Nanoparticles Electrochemically Grown on Gold Nanoislands Prefunctionalized by 1,4-phenylene Diisocyanide. *Electrochem. Solid-State Lett.* **2012**, *15*, K35−K39.
(29) Bicelli, L. P.; Bozzini, B.; Mele, C.; D'Urzo, L. A review of nanostructural aspects of metal electrodeposition. *Int. J. Electrochem. Sci.* **2008**, *3*, 356−408.
(30) Sohn, Y.; Pradhan, D.; Radi, A.; Leung, K. T. Interfacial Electronic Structure of Gold Nanoparticles on Si(100): Alloying versus Quantum Size Effects. *Langmuir* **2009**, *25*, 9557−9563.
(31) Kang, J.-S.; Jeong, Y.-K.; Kang, J.-G.; Zhao, L.; Sohn, Y.; Pradhan, D.; Leung, K. T. Observation of Mediated Cascade Energy Transfer in Europium-Doped ZnO Nanowalls by 1,10-Phenanthroline. *J. Phys. Chem. C* **2015**, *119*, 2142−2147.
(32) Zhou, J.; Acharya, D.; Camillone, N., III; Sutter, P.; White, M. G. Adsorption Structures and Electronic Properties of 1,4-Phenylene Diisocyanide on the Au(111) Surface. *J. Phys. Chem. C* **2011**, *115*, 21151−21160.
(33) Murphy, K. L.; Tysoe, W. T.; Bennett, D. W. A Comparative Investigation of Aryl Isocyanides Chemisorbed to Palladium and Gold: An ATR-IR Spectroscopic Study. *Langmuir* **2004**, *20*, 1732−1738.
(34) Garvey, M.; Kestell, J.; Abuflaha, R.; Bennett, D. W.; Henkelman, G.; Tysoe, W. T. Understanding and Controlling the 1,4-Phenylene Diisocyanide−Gold Oligomer Formation Pathways. *J. Phys. Chem. C* **2014**, *118*, 20899−20907.
(35) Lopez-Tobar, E.; Hara, K.; Izquierdo-Lorenzo, I.; Sanchez-Cortes, S. Plasmonic Effects of Phenylenediisocyanides Linked at Interparticle Junctions of Metal Nanoparticles. *J. Phys. Chem. C* **2015**, *119*, 599−609.
(36) Sohn, Y.; White, J. M. Solely σ-Atop Site Bonding of Phenyl Isocyanide on Au(111)? Comparison with on Cu(111). *J. Phys. Chem. C* **2008**, *112*, 5006−5013.
(37) Silien, C.; Lahaye, D.; Caffio, M.; Schaub, R.; Champness, N. R.; Buck, M. Electrodeposition of Palladium onto a Pyridine-Terminated Self-Assembled Monolayer. *Langmuir* **2011**, *27*, 2567−2574.
(38) Wang, A.-Q.; Liu, J.-H.; Lin, S. D.; Lin, T.-S.; Mou, C.-Y. Au−Cu Alloy nanoparticles confined in SBA-15 as a highly efficient catalyst for CO oxidation. *J. Catal.* **2005**, *233*, 186−197.
(39) Stapleton, J. J.; Daniel, T. A.; Uppili, S.; Cabarcos, O. M.; Naciri, J.; Shashidhar, R.; Allara, D. L. Self-Assembly, Characterization, and Chemical Stability of Isocyanide-Bound Molecular Wire Monolayers on Gold and Palladium Surfaces. *Langmuir* **2005**, *21*, 11061−11070.
(40) Zhao, L. Y.; Eldridge, K. R.; Sukhija, K.; Jalili, H.; Heinig, N. F.; Leung, K. T. Electrodeposition of Iron core-shell nanoparticles on a H-terminated Si(100) surface. *Appl. Phys. Lett.* **2006**, *88*, 033111.
(41) Sohn, Y.; Pradhan, D.; Kang, J.-S.; Leung, K. T. Nanoscale Architecture of Bimetallic Hybrid Fe−Au Nanostructures with and without 1, 4-Phenylene Diisocyanide Pre-functionalization. *RSC Adv.* **2015**, *5*, 31472−31478.
(42) Radi, A.; Pradhan, D.; Sohn, Y.; Leung, K. T. Nanoscale Shape and Size Control of Cubic, Cuboctahedral, and Octahedral Cu-Cu_2O Core-Shell Nanoparticles on Si(100) by One-Step, Templateless, Capping-Agent-Free Electrodeposition. *ACS Nano* **2010**, *4*, 1553−1560.

DOI: 10.1021/acs.langmuir.7b02705
Langmuir 2018, 34, 2849−2855